Journal of Structural Geology 33 (2011) 1312–1324

Contents lists available at ScienceDirect

Journal of Structural Geology

journal homepage: www.elsevier.com/locate/jsg

How do the properties of a pre-existing normal-fault population influence fault development during a subsequent phase of extension?

Alissa A. Henza [1,*], Martha Oliver Withjack, Roy W. Schlische

Department of Earth and Planetary Sciences, Rutgers University, Piscataway, NJ, 08544-8066, USA

ARTICLE INFO

Article history:
Received 14 March 2011
Received in revised form
21 June 2011
Accepted 30 June 2011
Available online 20 July 2011

Keywords:
Normal faults
Experimental modeling
Two-phase extension
Fault reactivation

ABSTRACT

We use scaled experimental (analog) models to investigate how the properties of a population of pre-existing normal faults influence fault development during a subsequent phase of extension. In the models, a homogeneous layer of wet clay undergoes two phases of extension whose extension directions differ by 45°. To vary the properties of the first-phase fault population, we vary the magnitude of the first-phase extension. As the magnitude of the first-phase extension increases, the number, average and maximum length, and average and maximum displacement of the first-phase normal faults increase. For a poorly developed first-phase fault population, new normal faults (which strike perpendicular to the second-phase extension direction) form during the second phase. For a well developed first-phase fault population, many first-phase normal faults are reactivated as oblique-slip faults during the second phase. New normal faults also form; these second-phase normal faults are shorter and have displacement maxima adjacent to the reactivated first-phase faults. They are less likely to cut the pre-existing first-phase faults than second-phase normal faults that form in models with a less developed first-phase fault population. In all models, pre-existing faults serve as nucleation sites for new faults. In models with a well developed first-phase fault population, the pre-existing faults also act as obstacles to the propagation of the second-phase normal faults. Fault geometries in the models vary considerably; parallel, zig-zag, or intersecting fault geometries develop depending on whether the first-phase fault population is poorly, moderately, or well developed, respectively.

1. Introduction

Many rift systems have undergone multiple phases of extension, commonly with differing extension directions (e.g., Badley et al., 1988; Sinclair, 1995; Boccaletti et al., 1998; Lepvrier et al., 2002; Huchon and Khanbari, 2003; Morley et al., 2004; Bellahsen et al., 2006). The fault geometries within these rift systems are varied and complex, characterized by faults with multiple trends and zig-zag or intersecting geometries. Recent experimental (analog) models with two phases of non-coaxial extension (Bonini et al., 1997; Keep and McClay, 1997; Dubois et al., 2002; Bellahsen and Daniel, 2005; Henza et al., 2010) show that the orientation of pre-existing normal faults significantly influences fault development during subsequent phases of extension. Specifically, (1) the likelihood of fault reactivation, (2) the magnitude and sense of slip of the reactivated faults, and (3) the attitude, number, and length of the new normal faults depend on the orientation of the first-phase faults relative to the second-phase extension direction.

Other properties of a pre-existing normal-fault population (i.e., the number, length, and displacement of faults) likely influence fault development during subsequent phases of extension. To better define this influence, we conducted a series of scaled experimental models with two phases of non-coaxial extension in which the magnitude of the first-phase extension varies. Single-phase models of orthogonal and oblique extension (e.g., Ackermann et al., 2001; Clifton and Schlische, 2001; Bellahsen et al., 2003) show that the number of normal faults, their average and maximum length, and their average and maximum displacement generally increase as the magnitude of extension increases. Thus, by varying the magnitude of the first-phase extension in our models, we also vary the properties of the first-phase fault population, allowing us to better understand the influence of these properties on fault development during the second phase of extension.

2. Experimental approach

2.1. Modeling materials

Wet clay and dry sand are the most common modeling materials used in scaled experimental models. Although the large-scale

* Corresponding author. Tel.: +1 281 888 4337.
E-mail address: ahenza@gmail.com (A.A. Henza).
[1] Present address: BHP Billiton Petroleum (Americas) Inc., 1360 Post Oak Boulevard, Houston, TX, USA 77057.

0191-8141/$ – see front matter © 2011 Elsevier Ltd. All rights reserved.
doi:10.1016/j.jsg.2011.06.010

deformation patterns are similar in clay and sand models with similar boundary conditions, the small-scale deformation differs in subtle, but important, ways (e.g., Withjack and Callaway, 2000; Eisenstadt and Sims, 2005; Withjack and Schlische, 2006). Fault zones are narrower in clay models (<0.1 mm) than in sand models (>1.0 mm). Deformation is more distributed in clay models (numerous minor to major normal faults and folds) than in sand models (mostly major normal faults). Finally, fault propagation and linkage are slower in clay models than in sand models, leading to the development of more relay ramps and more sinuous fault traces in clay models than in sand models. In this study, we selected wet clay as the modeling material to best capture the detailed evolution and interaction of faults during both phases of extension.

The wet clay in our models is similar to that used in previous modeling studies of extension (e.g., Withjack and Callaway, 2000; Eisenstadt and Sims, 2005; Withjack and Schlische, 2006; Henza et al., 2010). It is primarily composed of kaolinite particles (<0.005 mm in diameter) and water (~40% by weight) and has a density of 1.55–1.60 g cm^{-3}. Its coefficient of internal friction is 0.6 and its cohesive strength is ~50 Pa. The cohesion and coefficient of internal friction of wet clay are appropriate to ensure dynamic similarity between the models and nature (e.g., Withjack and Callaway, 2000; Henza et al., 2010).

2.2. Experimental set-up

Our experimental set-up resembles the set-up in previous models of single-phase and multiphase oblique extension (e.g., Withjack and Jamison, 1986; Tron and Brun, 1991; Bonini et al., 1997; Keep and McClay; 1997; Clifton et al., 2000; Henza et al., 2010). The base of the apparatus consists of an initially 8-cm-wide rubber sheet attached to two rigid sheets (one fixed and one mobile) (Fig. 1a). A 0.5-cm-thick layer of PDMS silicone polymer with a viscosity of about 10^4 Pa s, (Weijermars, 1986; ten Grotenhuis et al., 2002; S. Dixon, 1996, personal communication) overlies the rubber sheet. A layer of wet clay (60-cm wide, 68-cm long) covers the polymer layer, the fixed sheet, and the mobile sheet (Fig. 1b). The clay layer is 3.5-cm thick above the polymer layer and 4.0-cm thick above the sheets. The layer of silicone polymer decouples the clay layer from the rubber sheet, allowing the base of the clay layer to move vertically during deformation (Henza et al., 2010).

Table 1
Displacement and strain magnitudes for Models A–E. The maximum horizontal extension is calculated using Equation 9 in Withjack and Jamison (1986).

	Model A	Model B	Model C	Model D	Model E
Final magnitude of first-phase displacement (cm)	0	2.0	2.5	3.0	3.5
1st phase final maximum horizontal extension (percent)	0	21.7	27.2	32.8	38.4
Final magnitude of second-phase displacement (cm)	3.5	3.5	3.5	3.5	3.5
2nd phase final maximum horizontal extension (percent)	38.4	32.5	31.3	30.2	29.1

Using the notation of Withjack and Jamison (1986), α is the angle (measured clockwise) between the long axis of the rubber sheet and the displacement direction of the mobile sheet (Fig. 1c). Withjack and Jamison (1986) noted that the direction of maximum extension differs from the displacement direction except for $\alpha = 90°$; specifically, the direction of maximum extension (E) initially lies midway between the displacement direction and the normal to the long axis of the rubber sheet. Previous models of oblique extension (e.g., Withjack and Jamison, 1986; Tron and Brun, 1991; McClay and White, 1995; Clifton et al., 2000; Henza et al., 2010) and this study show that normal faults form if $45° \leq \alpha \leq 135°$. For other values of α, oblique-slip and/or strike-slip faults also develop. In this study, we use $\alpha_1 = 45°$ ($E_1 = 67.5°$) and $\alpha_2 = 135°$ ($E_2 = 112.5°$) (Fig. 1c), which is the maximum possible difference in displacement directions for which only normal faults develop (e.g., Henza et al., 2010). The displacement directions

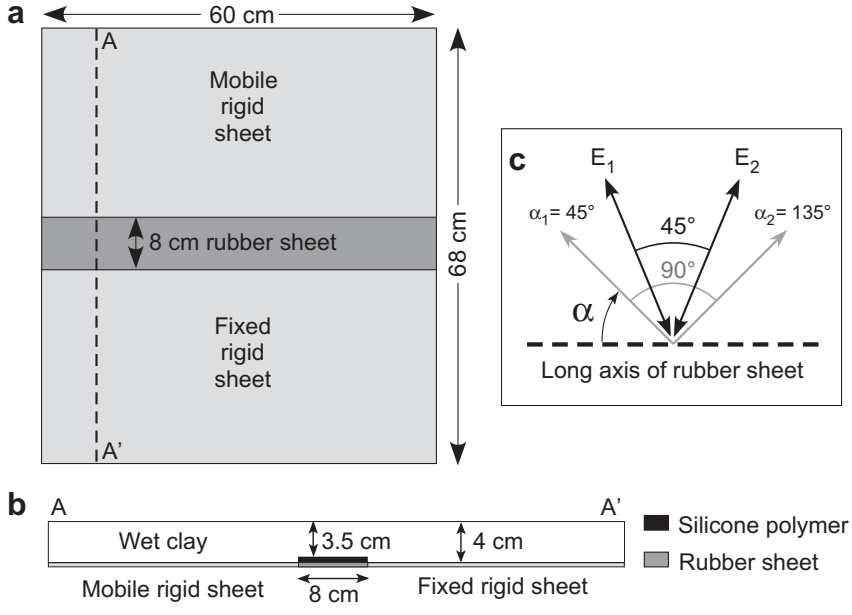

Fig. 1. Experimental set-up in (a) plan view and (b) cross-sectional view. (c) Displacement directions (gray arrows) and initial extension directions (black double-headed arrows). α is the angle measured clockwise from long axis of rubber sheet to displacement direction. α_1 defines the first-phase displacement direction, α_2 defines the second-phase displacement direction. E_1 and E_2 are the initial maximum extension directions for phase 1 and phase 2, respectively. The initial direction of the maximum extension lies halfway between the displacement direction and the normal to the long axis of the rubber sheet.

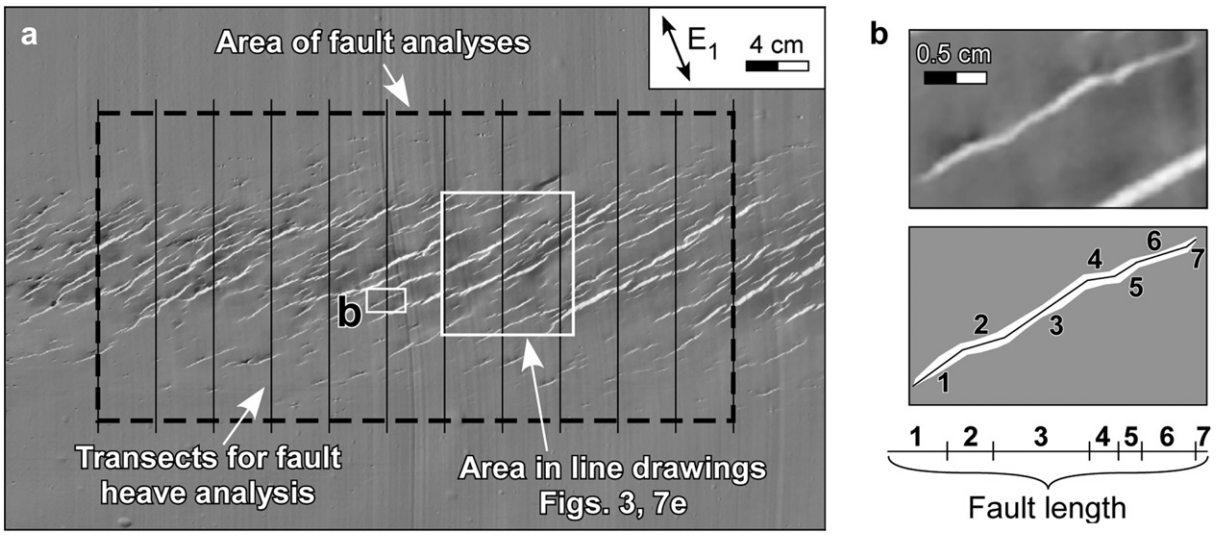

Fig. 2. Fault-analysis methods. (a) Photograph of Model E after first phase of extension showing area of fault analysis (black dashed box), area covered by line drawing of faults (white box), and transects used to determine fault heaves (solid black lines). E_1 is initial direction of maximum extension during first phase. Fault scarps dipping toward top of page appear bright; fault scarps dipping toward bottom of page appear dark. (b) Photograph (above) and line drawing (below) of normal fault from Model E after first phase of extension (see location in a). Line drawing shows fault heave (white area) and segmented line halfway between hanging-wall and footwall cutoffs. Each segment is straight with an orientation that differs from those of adjoining segments by at least 5°. The straight-line fit for this fault results in seven distinct segments with seven distinct orientations. We define individual fault length as the summed lengths of the segments.

during the first and second phases differ by 90°, whereas the initial directions of maximum extension differ by 45° (Fig. 1c).

All models (except for Model A; Table 1) undergo two phases of extension. During the first phase, the mobile sheet moves outward at 4 cm h^{-1} in a prescribed direction ($\alpha_1 = 45°$); the displacement magnitude ranges from 2 to 3.5 cm (Fig. 1c, Table 1). The magnitude of the maximum horizontal extension of the rubber sheet ranges from ~22% to ~38%. During the second phase, the mobile plate moves outward at a rate of 4 cm h^{-1} in a different prescribed direction ($\alpha_2 = 135°$); the displacement magnitude is 3.5 cm for all models.

2.3. Analyses

We use photographs of the top surface of the models to characterize the fault populations at the end of the first phase, midway through the second phase, and at the end of the second phase of extension. All analyses use only the central part of the models to avoid lateral edge effects (Fig. 2a). The offset of passive markers (e.g., superficial lines on the model surface) and the attitude of corrugations on fault surfaces (Maltman, 1987; Hancock and Barka, 1987; Granger et al., 2008) indicate the sense of slip of the faults.

	Model A	Model B	Model C	Model D	Model E
1st-phase displacement (cm)	0	2.0	2.5	3.0	3.5
Maximum horizontal extension (%)	0	21.7	27.1	32.8	38.4
Line drawings of fault heaves from top surface 4 cm	No 1st-phase extension	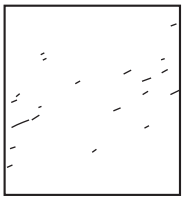	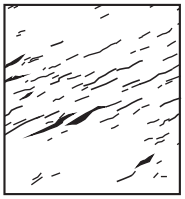	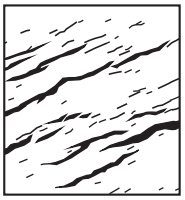	
Rose diagram scaled to summed lengths of fault segments (outside circle is 500 cm; bin size is 10°)	No 1st-phase extension			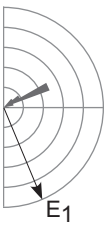	
Summed lengths of fault segments (cm)	0	53	245	344	541

Fig. 3. Properties of first-phase fault populations for Models A through E.

For each fault, we draw a segmented line midway between the hanging-wall and footwall cutoffs (Fig. 2b). Segments are straight, and their orientations differ from those of adjoining segments by at least 5°. We measure fault heaves perpendicular to fault strike for all faults that intersect 12 transects in the area of analysis (Fig. 2a). These data provide the number of fault segments, the length and orientation of each fault segment, the summed lengths of all fault segments, the length of individual faults (e.g., the summed lengths of fault segments for each fault; Fig. 2b), the heave of individual faults, and the 95th percentile length and heave of individual faults (see Clifton et al., 2000) at the end of the first phase of extension. The linkage of first-phase and second-phase faults makes identification of individual faults during the second phase problematic. Thus, for the second phase of extension, we determine only the number of fault segments, the length and orientation of each segment, the summed lengths of segments, the sense of slip on segments, and the number and type of interactions between intersecting first-phase and second-phase segments (i.e., cross-cutting, terminating). We group fault segment orientations into three categories: (1) those striking approximately perpendicular ($\pm 10°$) to the first-phase extension direction, (2) those striking approximately perpendicular ($\pm 10°$) to the second-phase extension direction (applicable only during the second phase of the models), and (3) all others (which we consider oblique to both extension directions). The sum of fault-segment lengths within each category reflects both the development and dominance of a fault population after the first and second phases of extension.

3. First-phase extension and fault-population characteristics

Normal faults form in the clay layer above the rubber sheet and silicone polymer during the first phase of extension ($\alpha_1 = 45°$) in Models B through E (Model A has no first-phase extension; Fig. 3). In cross section, these faults are narrow (<0.1 mm wide), well-defined zones of re-aligned clay particles (Fig. 4), similar to the shear zones described in Maltman (1987). Thus, once fault zones are established, they become permanent features of the clay layer. Most normal faults strike approximately perpendicular to the initial direction of maximum horizontal extension (Fig. 3). However, some segments are oblique to this direction; these segments are most likely related to the linkage of previously unconnected fault segments (e.g., Peacock and Sanderson, 1991; Dawers and Anders, 1995).

As the magnitude of the first-phase extension increases (i.e., from Model B to Model E), the number of fault segments, the summed lengths of fault segments, the number of individual faults, the average fault length and heave, and the 95th percentile of fault length and heave increase (Figs. 3 and 5). Specifically, for Model E relative to Model B, (1) the number of fault segments is approximately six times greater, and the number of individual faults is more than three times greater (Fig. 5a); (2) the average fault length is approximately three times greater, and the 95th percentile of fault length is more than six times greater (Fig. 5b); (3) the average fault heave is almost two times greater, and the 95th percentile of fault heave is more than two times greater (Fig. 5c). The ratio of average fault heave to length decreases as the magnitude of extension increases (Fig. 5d). The ratio of 95th percentile fault heave to length, however, differs only slightly for Models C, D, and E (Fig. 5d). Thus, the ratio of fault heave to length does not change significantly for the largest normal faults once the magnitude of extension exceeds ~25%.

The fault-population statistics, together with the map-view fault patterns (Fig. 3), show that the properties of the normal-fault populations differ significantly in Models B through E. Model B (22% extension) has a poorly developed first-phase fault population in which few normal faults are present. These faults are isolated, short, and have small heaves. The first-phase fault population is better developed in Model C (27% extension). More normal faults are present, and the largest normal faults are much longer than those in Model B (Fig. 5b). Model D (33% extension) has a well developed first-phase fault population. The largest normal faults are much longer and have much greater heave than those in Model C (Fig. 5b and c). Model E (38% extension) has a very well developed first-phase fault population. The average fault length and the 95th percentage fault length are much greater in Model E than in Model D (Fig. 5b).

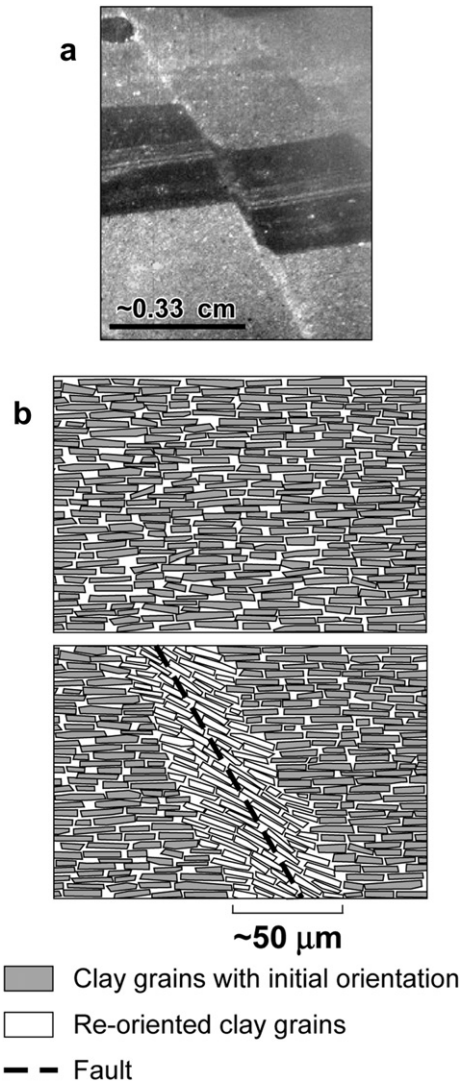

Fig. 4. Fault zones in clay models. (a) Thin section (crossed polars) of dried clay model with normal fault zones, which have different optical properties than surrounding unfaulted clay due to re-aligned mineral grains. (b) Sketch showing initial orientation of clay grains (top) and re-oriented clay grains in a fault zone (bottom).

The characteristics of the first-phase fault populations in our models are similar to those documented during the evolution of single-phase clay models of orthogonal (e.g., Ackermann et al., 2001; Bellahsen et al., 2003) and oblique (e.g., Clifton and Schlische, 2001) extension. These studies show that fault-population characteristics change as extension increases, reflecting changes in fault-growth processes (i.e., nucleation, propagation, linkage).The ratios of average fault heave to length (0.12–0.19) and ratios of the 95th percentile fault heave to length (0.06–0.17) for all of the first-phase fault populations in our models (Fig. 5d) are similar to those observed in natural fault populations (e.g., Kim and Sanderson, 2005).

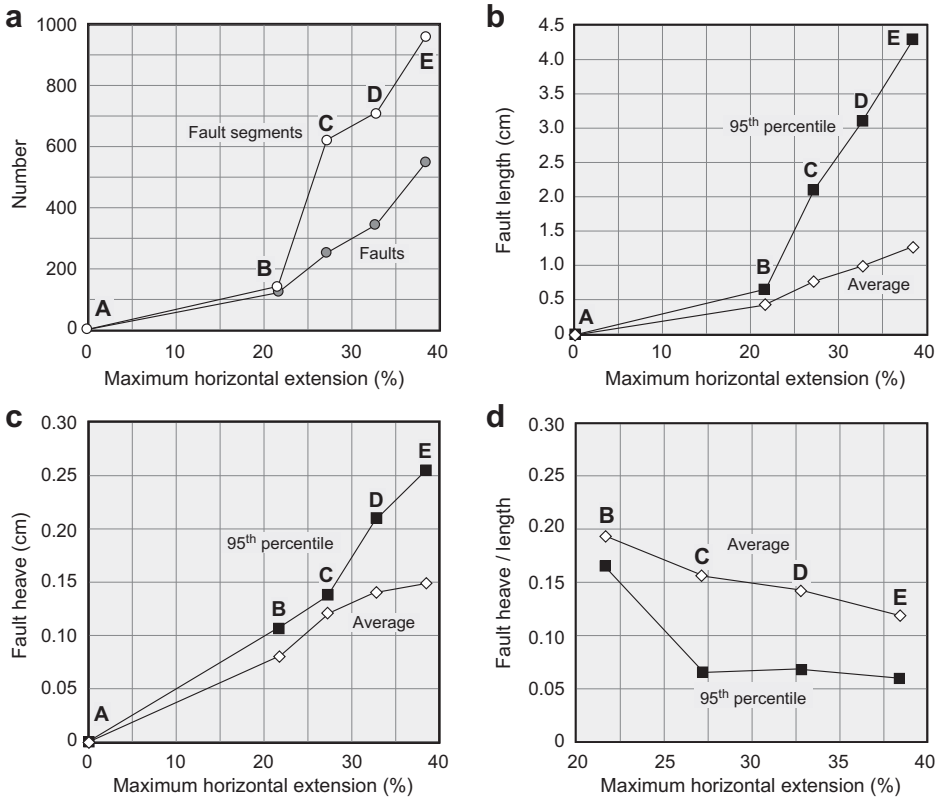

Fig. 5. Graphs showing properties of first-phase fault populations for Models A through E. (a) Number of fault segments and individual faults vs. magnitude of maximum horizontal extension. (b) Average and 95th percentile fault length vs. magnitude of maximum horizontal extension. (c) Average and 95th percentile fault heave vs. magnitude of maximum horizontal extension. (d) Heave to length ratios for average and 95th percentile values vs. magnitude of maximum horizontal extension.

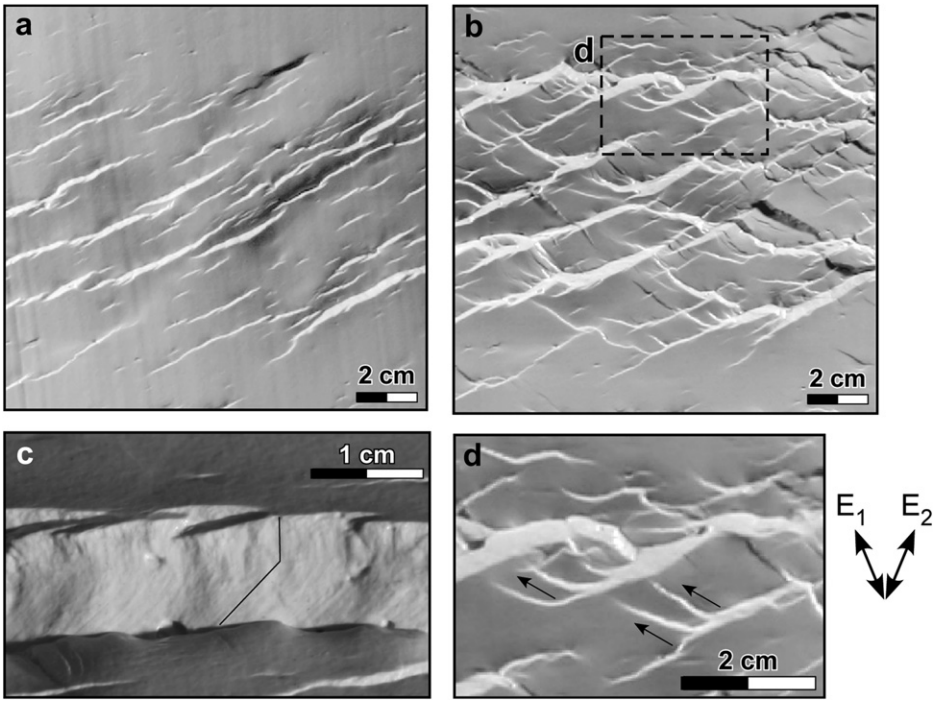

Fig. 6. Photographs of part of top surface of Model E at (a) end of first phase of extension and (b) end of second phase of extension. Faults dipping toward top of page appear bright; faults dipping toward bottom of page appear dark. (c) Close-up photograph of fault from Model E after second phase of extension. Two sets of corrugations are present on fault surface showing that fault had normal slip during first phase of extension and oblique slip during second phase of extension. (d) Close-up photograph showing second-phase faults initiating and propagating outward from tips and center of first-phase faults (location in b). Arrows indicate direction of second-phase fault propagation. E_1 and E_2 are the initial maximum extension directions for phase 1 and phase 2, respectively.

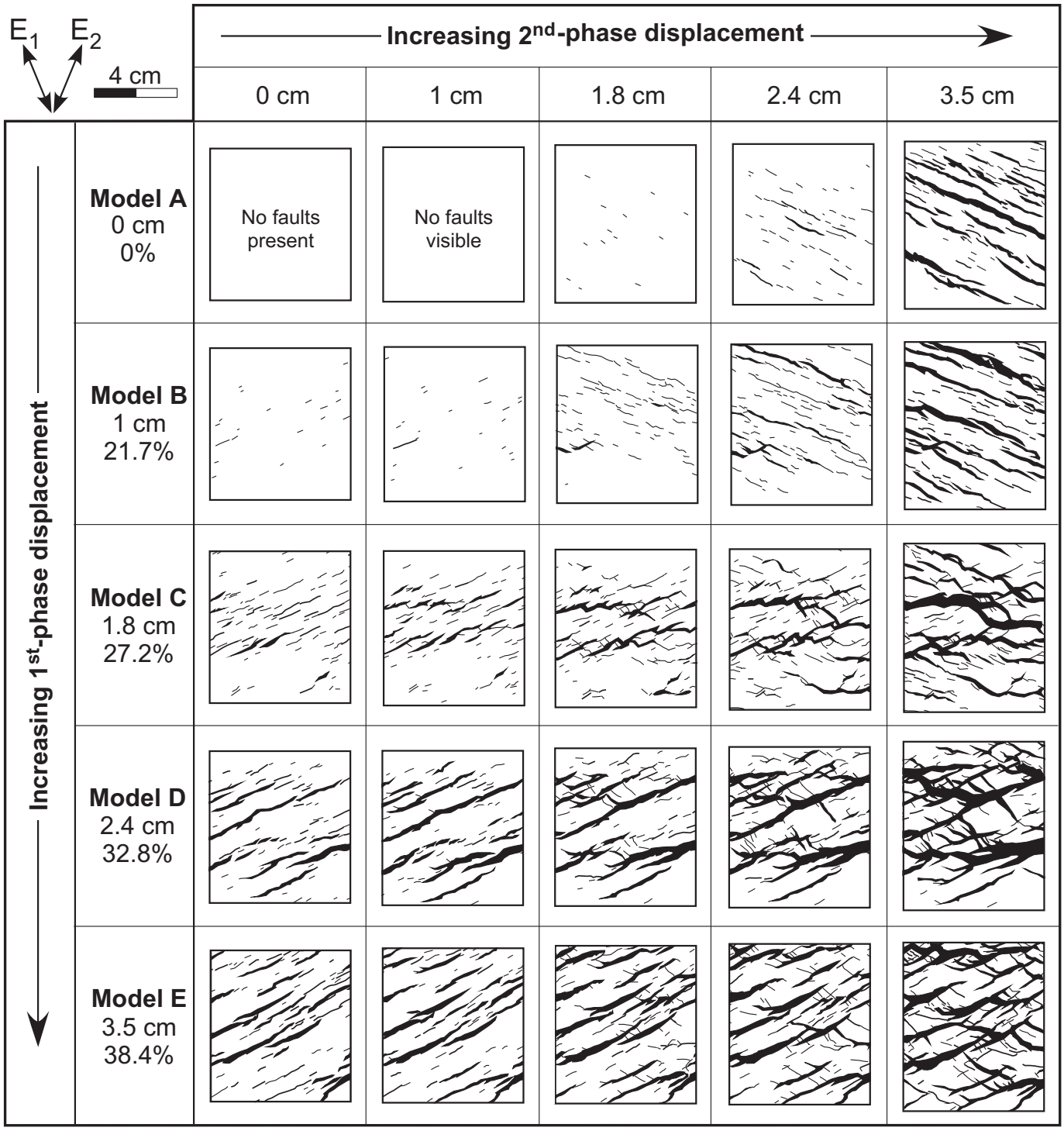

Fig. 7. Line drawings of fault heaves for Models A through E for increasing displacement during second-phase of extension. Numbers below model names show magnitude of displacement and percent extension during first phase of extension. Line drawings are from same locations as those in Fig. 3. E_1 and E_2 are the initial maximum extension directions for phase 1 and phase 2, respectively.

4. Second-phase extension and fault development

4.1. Reactivation of first-phase faults and development of new faults

First-phase faults are reactivated with oblique-slip (normal and right-lateral strike-slip components) during the second phase of extension in all models (Figs. 6 and 7). As the magnitude of the second-phase extension increases, new normal faults form in all models (Figs. 6 and 7). The strike of the new normal faults (Fig. 8) ranges from orthogonal to oblique to the second-phase extension direction and is oblique to the pre-existing faults (Henza et al., 2010). Midway through the second phase, the summed lengths of fault segments approximately ($\pm 10^{\circ}$) perpendicular to the second-phase extension direction are greater in Models B through E (with

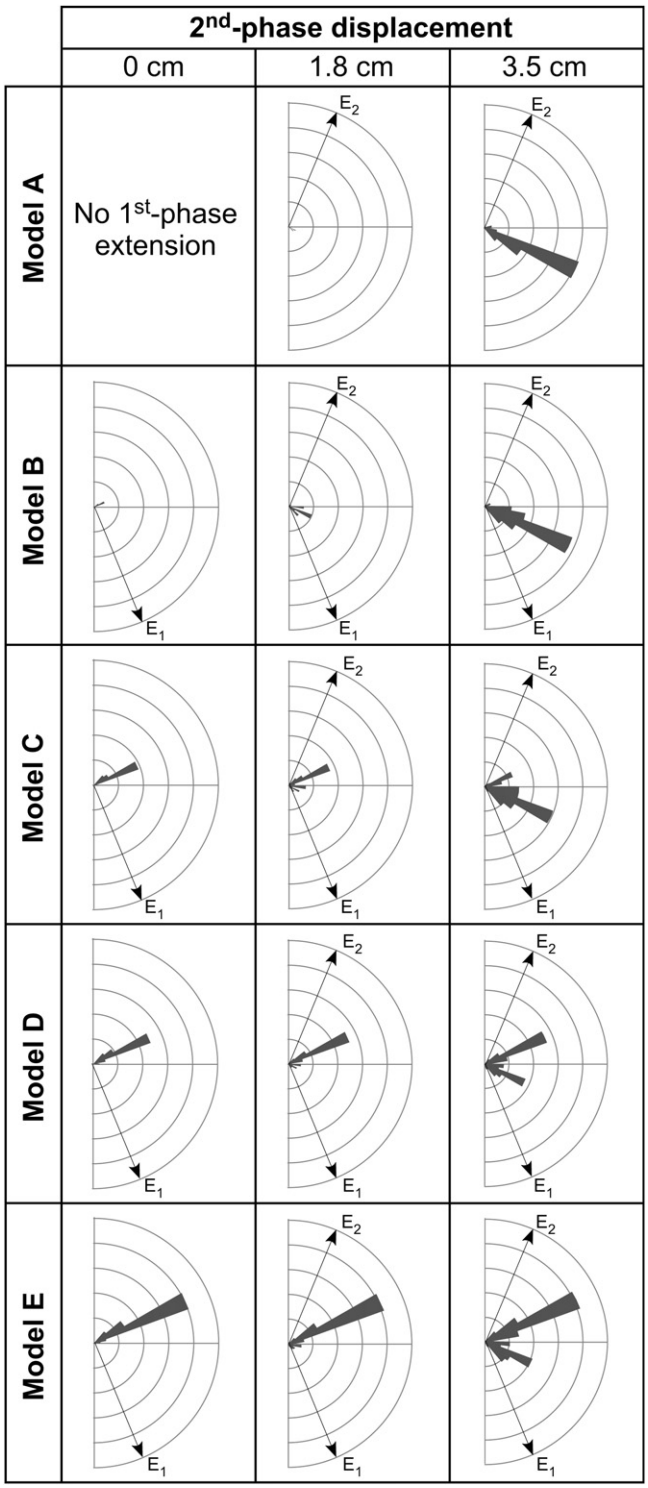

Fig. 8. Rose diagrams showing orientations of fault segments at start of second phase of extension (0 cm), midway through second phase of extension (1.8 cm), and at end of second phase of extension (3.5 cm). Arrows on rose diagrams show initial directions of maximum horizontal extension for first and second phases of extension (E_1 and E_2). Bin size for rose diagrams is 10°; outside circle of rose diagrams is 500 cm.

pre-existing fault populations) than in Model A (with no pre-existing faults) (Figs. 7 and 9). At the end of phase two, however, the summed lengths of fault segments approximately (±10°) perpendicular to the second-phase extension direction is greatest in the models with the least developed first-phase fault population (i.e., Models A and B) and least in models with the most developed first-phase fault population (i.e., Models D and E) (Figs. 7 and 9). Generally, the new second-phase faults are significantly shorter than faults that form under identical conditions without a pre-existing fault fabric (Fig. 7). The summed lengths of fault segments perpendicular to the first-phase extension direction is relatively constant during the second phase of extension, indicating that the first-phase faults do not significantly lengthen during the second phase of extension (Fig. 9).

4.2. Fault interactions

The interactions of the first-phase and second-phase faults during the second phase of extension depend on the properties of the first-phase fault population. In Model B (with a poorly developed first-phase fault population), the second-phase normal faults propagate along strike (Fig. 7). They link with other second-phase normal faults, but interactions with first-phase faults are limited (Fig. 7). In Models C through E (with better developed first-phase fault populations), many of the second-phase normal faults initiate at first-phase faults and propagate away from them (Fig. 6d). The second-phase normal faults initiate at both the tips and the center of the first-phase faults. The displacement on these second-phase normal faults is generally greatest adjacent to the pre-existing first-phase faults from which they initiate (Figs. 6d and 7), unlike many normal faults where displacements are greatest near the center of the faults (e.g., Walsh and Watterson, 1987) (see examples in Fig. 3).

As new normal faults propagate along strike, they commonly link with, cut across, or terminate against pre-existing first-phase faults. Linkage of the first-phase and second-phase faults creates faults with zig-zag geometries (Figs. 7 and 10). These composite faults have oblique-slip segments associated with the reactivated first-phase faults (Fig. 6c) and normal-slip segments associated with the new second-phase faults. They are best developed in Model C (with the moderately developed first-phase fault population) (Fig. 10). In Model C, the sum of fault-segment lengths striking approximately perpendicular to the first-phase extension direction decreases with increasing second-phase displacement magnitude (Fig. 9), reflecting the linkage and later obliteration of many first-phase faults by the new fault population.

In addition to linking with first-phase faults, many second-phase faults cut across or originate and/or terminate at the first-phase faults, creating intersecting fault geometries (Fig. 11). These geometries are best developed in Models D and E (with a well developed first-phase fault population) (Fig. 7). The number of second-phase faults that cut and offset first-phase faults and the number of second-phase faults that originate and/or terminate at first-phase faults depend on the properties of the first-phase fault population (Fig. 12). Cross-cutting interactions are greater than originating/terminating interactions in all models, regardless of the properties of the first-phase fault population. However, the percentage of fault interactions which are cross-cutting decreases as the magnitude of the first-phase extension increases (Fig. 12b).

5. Discussion

5.1. Implications of modeling results

Although Models A through E have identical kinematic histories during the second phase (i.e., the traced paths of surface particles are identical during the second phase of extension) (Fig. 13a), their second-phase fault patterns differ considerably. In models with a poorly developed first-phase fault population (Models A and B), the second-phase normal faults are longer and

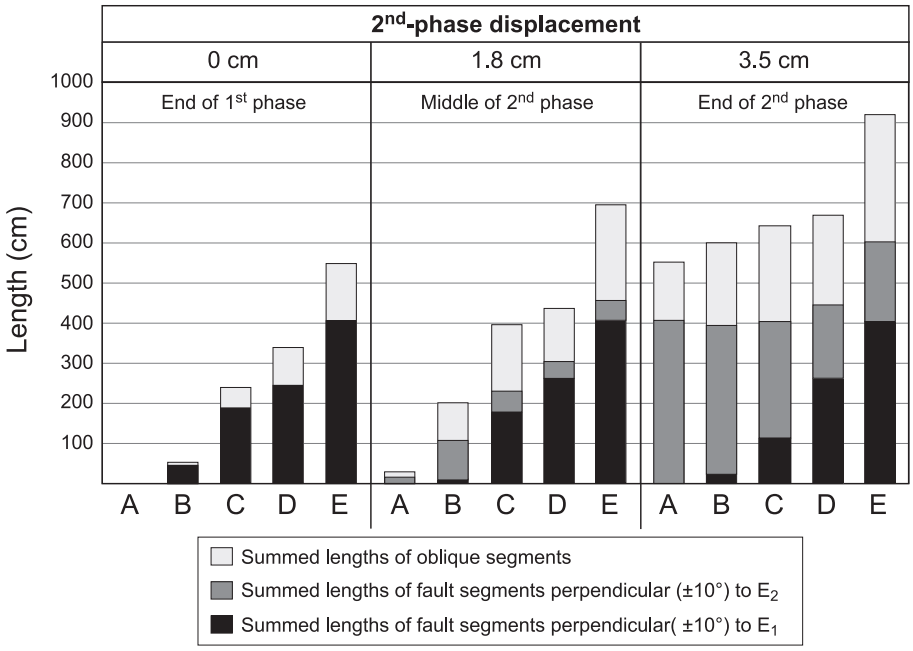

Fig. 9. Graph of summed lengths of fault segments at end of first phase of extension, midway through second phase of extension, and at end of second phase of extension for all models.

have more displacement than the reactivated first-phase faults, producing parallel fault geometries (Fig. 13). In models with a moderately developed first-phase fault population (Models C and D), many of the second-phase normal faults link with reactivated first-phase faults, producing zig-zag fault geometries (Fig. 13). In models with a well developed first-phase fault population (Models D and E), many of the second-phase normal faults cut across or originate and/or terminate at reactivated first-phase faults, producing intersecting fault geometries (Fig. 13). Thus, identical kinematic histories can produce very different fault geometries, depending on the properties of the pre-existing zones of weakness.

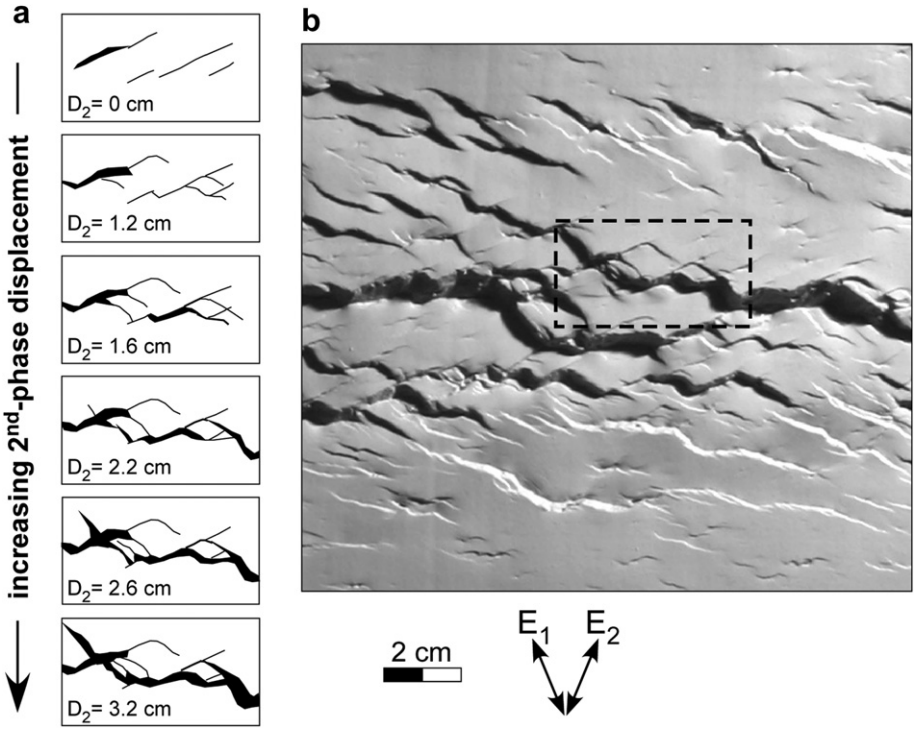

Fig. 10. Line drawings (a) and photograph (b) of Model C during second phase of extension. Line drawings, based on photographs of top surface of the model for increasing values of the second-phase displacement, show linkage of first-phase and second-phase faults and development of zig-zag fault geometry. Photograph shows top surface of model after 3.5 cm of second-phase displacement and location of final line drawing in a. Fault scarps dipping toward top of page appear bright; fault scarps dipping toward bottom of page appear dark. E_1 and E_2 are the initial maximum extension directions for phase 1 and phase 2, respectively.

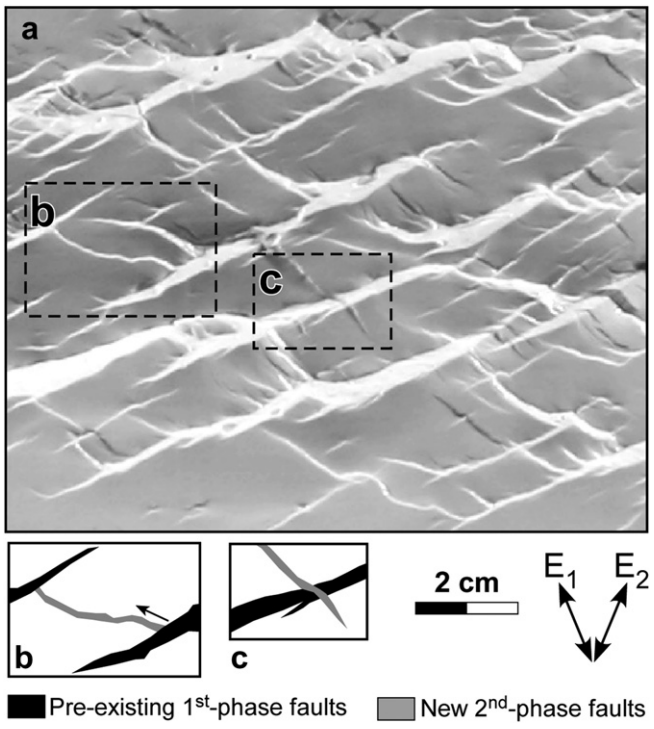

Fig. 11. Examples of cross-cutting and terminating fault interactions. (a) Photograph of part of top surface of Model E at end of second phase of extension. Faults dipping toward top of page appear bright; faults dipping toward bottom of page appear dark. E_1 and E_2 are the initial maximum extension directions for phase 1 and phase 2, respectively. (b) Line drawing showing new second-phase fault terminating against pre-existing first-phase faults. The new second-phase fault originates at one first-phase fault, propagates outward (direction indicated by arrow), and terminates against another first-phase fault. (c) Line drawing showing new second-phase fault cutting and offsetting pre-existing first-phase fault.

The dominance of one fault trend relative to another fault trend does not necessarily reflect the relative magnitudes of displacement during the two phases of extension. For example, the magnitude of displacement is identical during the first and second phases of extension in Model E. At the end of the experiment, however, the summed lengths of the first-phase fault segments (i.e., those that are perpendicular ($\pm 10^\circ$) to the first-phase extension direction) is approximately twice that of the second-phase fault segments (i.e., those that are perpendicular ($\pm 10^\circ$) to the second-phase extension direction) (Fig. 13c).

Previous workers have shown that faults created during an early episode of extension can affect fault development during subsequent episodes of extension by localizing strain and promoting new fault development (e.g., Meyer et al., 2002; Walsh et al., 2002) or, alternatively, by acting as obstacles and limiting the propagation and growth of new normal faults (e.g., Færseth et al., 1997; Færseth and Ravnås, 1998). In Models B through E, the first-phase faults serve as nucleation sites for second-phase normal faults, with new faults emanating from the tips and centers of the pre-existing faults (Fig. 6d). In Models C through E (with well developed first-phase fault populations), the first-phase faults also act as lateral obstacles, limiting the propagation and growth of the second-phase normal faults (Fig. 11b). Thus, our models suggest that even a poorly developed pre-existing fault population can promote the formation of new faults, but only a moderate- to well-developed fault population can limit the lateral (along-strike) propagation of new faults.

Although the models show that multiple episodes of extension can produce fault patterns with multiple fault trends and a variety of fault geometries, other geologic processes can produce similar fault patterns. For example, the reactivation of pre-existing zones of weakness that pre-date extension (e.g., Schumacher, 2002; Morley et al., 2004), the hard linkage of faults (e.g., Trudgill and Cartwright, 1994; Clifton et al., 2000; Schlische et al., 2002), and three-dimensional strain states (e.g., Reches, 1978, 1988; Krantz, 1988) can produce fault patterns with multiple fault trends during a single phase of extension. Thus, fault patterns alone are insufficient to identify multiple phases of extension. An understanding of the geologic history prior to extension (i.e., identify any pre-existing zones of weakness) and the timing of fault activity (using cross-cutting relationships, overprinted slickenlines, and growth beds) are both necessary.

5.2. Gulf of Aden rift system

As noted in Section 1, many rift systems have undergone multiple phases of extension, commonly with differing extension directions. We next apply our modeling results to the fault patterns in the Gulf of Aden rift system. We selected this rift system because it is well studied (e.g., Lepvrier et al., 2002; Huchon and Khanbari, 2003; Fournier et al., 2004; Bellahsen et al., 2006) and because the two proposed extension directions differ by about the same magnitude as those in our models.

In the eastern Gulf of Aden, rifting began during the Oligocene and continued until the onset of seafloor spreading during the

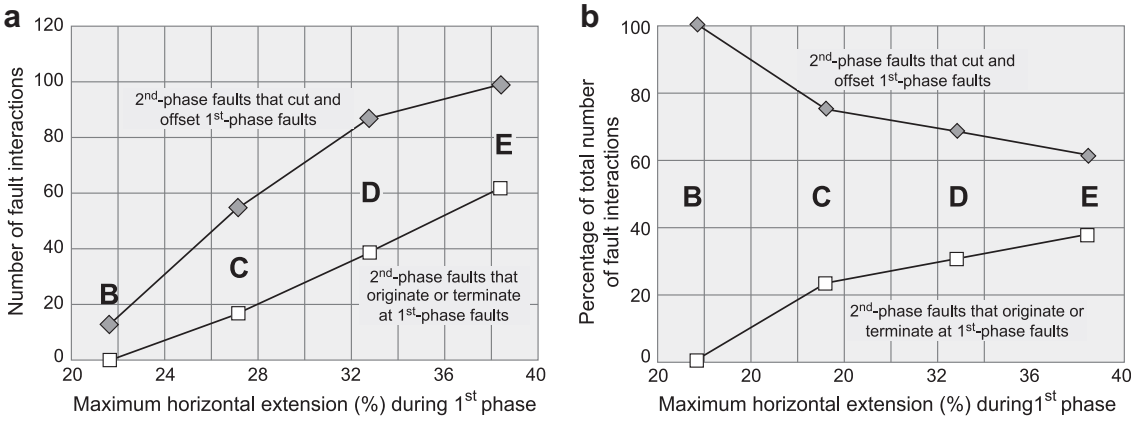

Fig. 12. (a) Graph showing number of cross-cutting and originating and/or terminating fault interactions at end of second phase of extension vs. magnitude of maximum horizontal extension during first phase of deformation for Models B through E. (b) Graph showing percentage of total number of fault interactions for the two types of interactions vs. magnitude of maximum horizontal extension during first phase of deformation for Models B through E.

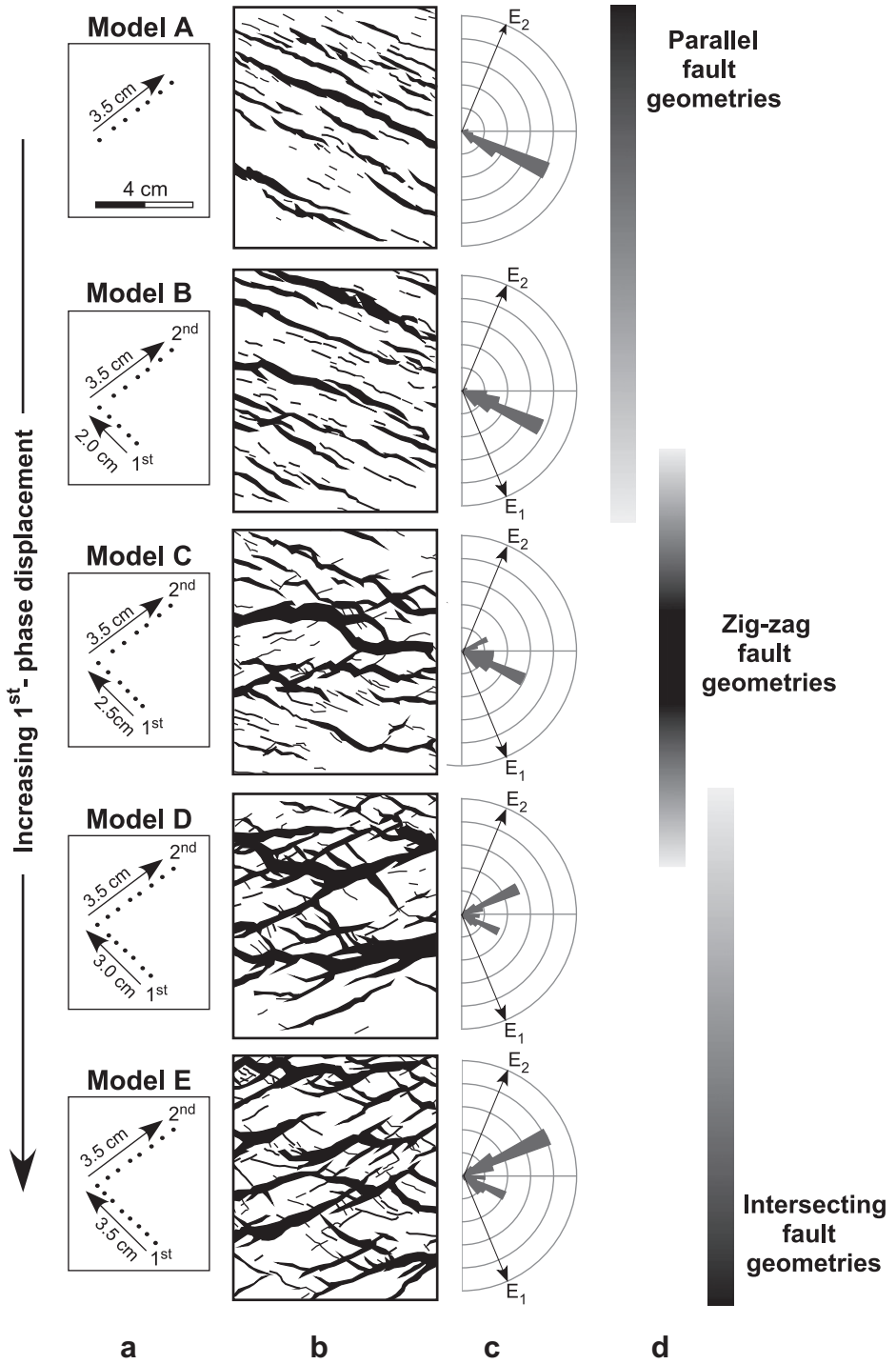

Fig. 13. Relationship between fault patterns and kinematics. (a) Representative displacement paths of surface particles relative to fixed camera/rigid sheet reference frame during first and second phases of extension. (b) Line drawings of fault heaves after second phase of extension. (c) Rose diagrams of fault segment orientations after second phase of extension (right column) for all models. Rose diagrams are scaled to summed lengths of fault segments. Arrows on rose diagrams show initial extension directions for each phase (E_1 and E_2). Bin size for rose diagrams is 10°; outside circle of rose diagrams equals 500 cm. (d) Types of fault geometries after second phase of extension.

Miocene (e.g., Lepvrier et al., 2002; Huchon and Khanbari, 2003). The WSW-trending rift system consists of a series of W- to WNW-trending basins that are now preserved on the conjugate continental margins of Arabia and Somalia (Fig. 14a). Oceanic transform faults and fracture zones show that the displacement direction of Arabia relative to Somalia was ~025°, highly oblique to the trend of the Gulf of Aden (~075°) (Fig. 14a). Thus, the Gulf of Aden rift system is an example of an oblique rift system where the relative displacement direction of opposite sides of the rift system was oblique to the trend of the rift system (Laughton et al., 1970; Girdler and Styles, 1978; Chase, 1978; Cochran, 1981; Withjack and Jamison, 1986).

At the map scale, two fault sets are common on the northern margin of the Gulf of Aden: a W- to WNW-striking set and a NE- to ENE-striking set (Fig. 14b and d). The interaction of these fault sets has produced parallel, intersecting, and zig-zag fault geometries.

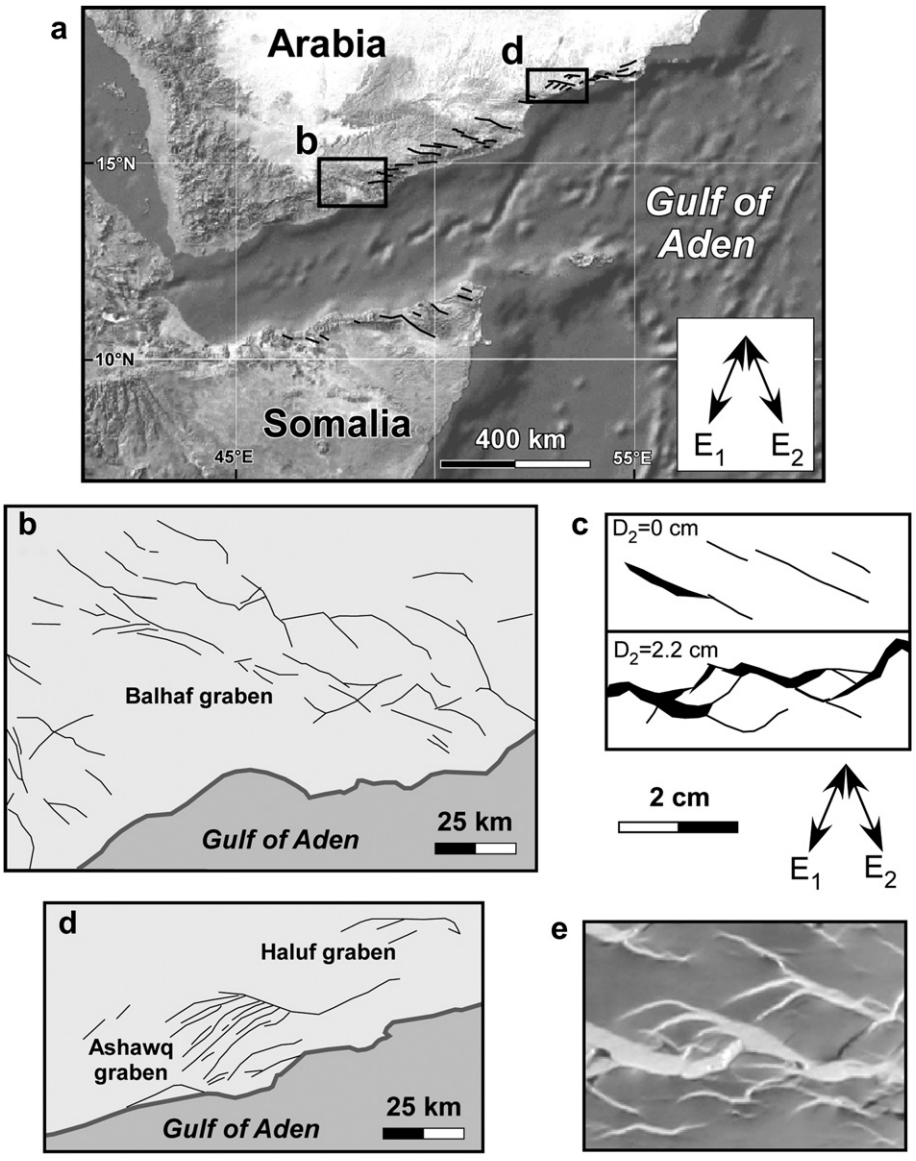

Fig. 14. (a) Bathymetry and topography of Gulf of Aden region (from http://energy.ihs.com/) showing NE-striking oceanic transform faults and fracture zones and major faults (black lines) on Arabian and Somalian continental margins (after Platel and Roger, 1989; Fantozzi and Sgavetti, 1998) and extension directions proposed by Lepvrier et al. (2002) and Huchon and Khanbari (2003). (b) Major faults near Balhaf graben (after Huchon and Khanbari, 2003). Location shown in (a). (c) Line drawings of part of Model C after first phase of extension (top) and after 2.2 cm of displacement during second phase of extension (bottom), flipped to match inferred extension directions in Gulf of Aden. (d) Major faults near Ashawq graben (after Lepvrier et al., 2002). Location shown in (a). (e) Photograph of top surface of Model E after second phase of extension. Image flipped to match inferred extension directions in Gulf of Aden. E_1 and E_2 are the initial maximum extension directions for phase 1 and phase 2, respectively.

For example, a zig-zag fault geometry occurs north of the Balhaf graben (Fig. 14b), whereas parallel and intersecting fault geometries occur within the Ashawq graben (Fig. 14d). Analyses of small-scale fault populations (Lepvrier et al., 2002; Huchon and Khanbari, 2003; Fournier et al., 2004; Bellahsen et al., 2006) suggest that two phases of extension (trending ~200° and ~160°) affected the northern margin of the Gulf of Aden during the Cenozoic rifting (Fig. 14a). The angle between these proposed extension directions is ~40; in our models, the angle is 45°. Limited geologic evidence suggests that the 200° extension preceded the 160° extension (Lepvrier et al., 2002; Huchon and Khanbari, 2003; Bellahsen et al., 2006), although Fournier et al. (2004) question this interpretation.

Although the angle between the two extension directions was the same for the northern margin of the Gulf of Aden, the fault geometries vary considerably. Our modeling results suggest that one factor that can produce these spatial variations in fault geometries is variations in the degree of development of the first-phase fault population. For example, if the first-phase fault population is poorly developed (i.e., few first-phase normal faults exist and are short and have small displacements), then the second-phase normal faults are more likely to be long and parallel, striking perpendicular to the second-phase extension direction. If the first-phase fault population is moderately well developed, then the second-phase normal faults are more likely to link with the first-phase faults, producing zig-zag fault geometries (Fig. 14d). If the first-phase fault population is well developed (i.e., first-phase faults are long and have large displacements), then the second-phase normal faults are likely to propagate from the tips and center of the first-phase faults producing intersecting fault geometries (Fig. 14e). Many of the NE-striking faults in the Gulf of Aden rift system appear to emanate from the tips or

centers of WNW-striking faults (Fig. 14d). Thus, the modeling results (Fig. 14e) suggest that the WNW-striking faults pre-date the NE-striking faults. Unless the WNW-striking faults are the result of a Mesozoic or older deformational episode, the 200° extension likely occurred before the 160° extension as suggested by Lepvrier et al. (2002) and Huchon and Khanbari (2003). Bellahsen et al. (2006), using the results of sand models of fault reactivation by Bellahsen and Daniel (2005) and field observations from the Gulf of Aden rift system, also support the hypothesis that the 200° extension predates the 160° extension.

6. Summary and conclusions

We use scaled experimental (analog) models to investigate how the properties of a normal-fault population that forms during one phase of extension affect fault development during a subsequent phase of extension. In our models, the first-phase and second-phase extension directions differ by 45°. We vary the properties of the first-phase normal-fault population by varying the magnitude of the first-phase extension. As the magnitude of the first-phase extension increases, the number of normal faults, the average fault length and heave, and the 95th percentile of fault length and heave increase. Thus, the degree of development of the first-phase fault population varies in our models from poorly developed (i.e., a few, short, isolated normal faults with small displacements) to well developed (i.e., numerous, large, linked normal faults with large displacements). The modeling results show the following:

1. First-phase faults are reactivated (with oblique-slip) and new normal faults form during the second phase of extension in all models, regardless of the degree of development of the first-phase fault population. The new normal faults strike approximately perpendicular to the second-phase extension direction.
2. Fault patterns in the models belong to one of three categories: (i) reactivated first-phase faults are dominant, (ii) second-phase normal faults are dominant, and (iii) neither first-phase faults nor second-phase faults are dominant. The dominance of first-phase faults relative to second-phase faults depends on the magnitude of the extension during both phases of deformation. It does not, however, necessarily reflect the relative magnitudes of extension during the two phases of deformation.
3. The degree of development of the first-phase fault population strongly influences the fault geometries that develop during the second phase of extension. If the first-phase fault population is poorly developed, then a series of long, parallel normal faults form during the second phase of extension. If the first-phase fault population is moderately developed, then many of the new normal faults link with the reactivated first-phase faults, forming composite faults with zig-zag geometries. If the first-phase fault population is well developed, then most of the new normal faults intersect the reactivated first-phase faults either by cutting across them or by originating/terminating at them.
4. Cross-cutting interactions are greater than originating/terminating interactions in all models, regardless of the degree of development of the first-phase fault population. The relative importance of cross-cutting interactions, however, decreases as the degree of development of the first-phase fault population increases.
5. The degree of development of the first-phase fault population influences the lengths and the locations of displacement maxima of the second-phase normal faults. Specifically, the second-phase normal faults are longer and their displacement maxima are nearer the fault centers if the first-phase fault population is poorly developed, whereas the second-phase normal faults are shorter and their displacement maxima are nearer one of the fault tips if the first-phase fault population is well developed.
6. The first-phase fault population promotes the formation of new normal faults during the second phase of extension in all models, even those with a poorly developed first-phase fault population. In contrast, the first-phase fault population limits the lateral (along-strike) growth of new faults only in models with a moderately to well developed fault population.
7. The parallel, intersecting, and zig-zag fault geometries observed on the margin of the Gulf of Aden are similar to those observed in our models, suggesting that the degree of development of the first-phase fault population in the Gulf of Aden varied along the margin.

Acknowledgments

We thank M. Durcanin, I. Sinclair, J. McIntyre, and N. Destro for valuable discussions and insights about modeling and fault interactions, H. Vora for his assistance in the laboratory, and M. Bonini, N. Dawers, and W. Dunne for their helpful reviews. We also thank the National Science Foundation (EAR-0838462 and EAR-0408878), Husky Energy, and Petrobras for their support of our research.

References

Ackermann, R.V., Schlische, R.W., Withjack, M.W., 2001. The geometric and statistical evolution of normal fault systems: an experimental study of the effects of mechanical layer thickness on scaling laws. Journal of Structural Geology 23, 1803–1819.

Badley, M.E., Price, J.D., Dahl, C.R., Agdestein, T., 1988. The structural evolution of the northern Viking Graben and its bearing upon extensional models of basin formation. Journal of the Geological Society, London vol. 145, 455–472.

Bellahsen, N., Daniel, J.M., 2005. Fault reactivation control on normal fault growth: an experimental study. Journal of Structural Geology 27, 769–780.

Bellahsen, N., Daniel, J.M., Bollinger, L., Burov, E., 2003. Influence of viscous layers on the growth of normal faults: insights from experimental and numerical models. Journal of Structural Geology 25, 1471–1485.

Bellahsen, N., Fournier, M., d'Acremont, E., Leroy, S., Daniel, J.M., 2006. Fault reactivation and rift localization: Northeastern Gulf of Aden margin. Tectonics 25. doi:10.1029/2004TC001626.

Boccaletti, M., Bonini, M., Mazzuoli, R., Abebe, B., Piccardi, L., Tortrici, L., 1998. Quaternary oblique extensional tectonics in the Ethiopian rift (Horn of Africa). Tectonophysics 287, 97–116.

Bonini, M., Souriot, T., Boccaletti, M., Brun, J.P., 1997. Successive orthogonal and oblique extension episodes in a rift zone: laboratory experiments with application to the Ethiopian Rift. Tectonics 16, 347–362.

Chase, C.G., 1978. Plate kinematics: the America, East Africa, and the rest of the world. Earth and Planetary Science Letters 37, 355–368.

Clifton, A.E., Schlische, R.W., Withjack, M.O., Ackermann, R.V., 2000. Influence of rift obliquity on fault-population systematics: results of clay modeling experiments. Journal of Structural Geology 22, 1491–1509.

Clifton, A.E., Schlische, R.W., 2001. Nucleation, growth and linkage of faults in oblique rift zones: results from experimental clay models and implications for maximum fault size. Geology 29, 455–458.

Cochran, J.R., 1981. The Gulf of Aden: structure and evolution of a young ocean basin and continental margin. Journal of Geophysical Research 86, 263–287.

Dawers, N.H., Anders, M.H., 1995. Displacement-length scaling and fault linkage. Journal of Structural Geology 17, 607–614.

Dubois, A., Odonne, F., Massonnat, G., Lebourg, T., Fabre, R., 2002. Analogue modelling of fault reactivation: tectonic inversion and oblique remobilization of grabens. Journal of Structural Geology 24, 1741–1752.

Eisenstadt, G., Sims, D., 2005. Evaluating sand and clay models: do rheological differences matter? Journal of Structural Geology 27, 1399–1412.

Færseth, R.B., Knudsen, B.-E., Liljedahl, T., Midbøe, P.S., Søderstrøm, B., 1997. Oblique rifting and sequential faulting in the Jurassic development of the northern North Sea. Journal of Structural Geology 19, 1285–1302.

Færseth, R.B., Ravnås, R., 1998. Evolution of the Oseberg fault-block in context of the northern North Sea structural framework. Marine and Petroleum Geology 15, 467–490.

Fantozzi, P.L., Sgavetti, M., 1998. Tectonic and sedimentary evolution of the eastern Gulf of Aden continental margins: new structural and stratigraphic data from Somalia and Yemen. In: Purser, B.H., Bosence, D.W.J. (Eds.), Sedimentation and

Tectonics of Rift Basins: Red Sea– Gulf of Aden. Chapman & Hall, London, pp. 56–76.
Fournier, M., Bellahsen, N., Fabbri, O., Gunnell, Y., 2004. Oblique rifting and segmentation of the NE Gulf of Aden Passive margin. Geochemistry, Geophysics, and Geosystems 11. doi:10.1029/2004GC000731.
Girdler, R.W., Styles, P., 1978. Seafloor spreading in the western Gulf of Aden. Nature 271, 615–617.
Granger, A.B., Withjack, M.O., Schlische, R.W., 2008. Fault surface corrugations: insights from scaled experimental models of extension. In: "Fault Zones: Structure, Geomechanics, and Fluid Flow" Conference. Geological Society of London, September 2008, Abstracts Volume, p. 38.
Hancock, P.L., Barka, A.A., 1987. Kinematic indicators on active normal faults in western Turkey. Journal of Structural Geology 9, 573–584.
Henza, A.A., Withjack, M.O., Schlische, R.W., 2010. Normal-fault development during two phases of non-coaxial extension: an experimental study. Journal of Structural Geology 32, 1656–1667.
Huchon, P., Khanbari, K., 2003. Rotation of the syn-rift stress field of the northern Gulf of Aden margin, Yemen. Tectonophysics 364, 147–166.
Keep, M., McClay, K.R., 1997. Analogue modeling of multiphase rift systems. Tectonophysics 273, 239–270.
Kim, Y.-S., Sanderson, D.J., 2005. The relationship between displacement and length of faults: a review. Earth-Science Reviews 68, 317–334.
Krantz, R.W., 1988. Multiple fault sets and three-dimensional strain: Theory and application. Journal of Structural Geology 10, 225–237.
Laughton, A.S., Whitmarsh, R.B., Jones, M.T., 1970. The evolution on the Gulf of Aden. Philosophical Transactions of the Royal Society of London Series A vol. 267, 227–266.
Lepvrier, C., Fournier, M., Bérard, T., Roger, J., 2002. Cenozoic extension in coastal Dhofar (southern Oman): implications on the oblique rifting on the Gulf of Aden. Tectonophysics 357, 279–293.
Maltman, A.J., 1987. Shear zones in argillaceous sediments- an experimental study. In: Jones, M.E., Preston, R.M.F. (Eds.), Deformation of Sediments and Sedimentary Rocks. Geological Society (London) Special Publication, vol. 29, pp. 77–87.
McClay, K.R., White, M.J., 1995. Analogue modeling of orthogonal and oblique rifting. Marine and Petroleum Geology 12, 137–151.
Meyer, V., Nicol, C., Childs, C., Walsh, J.J., Watterson, J., 2002. Progressive localisation of strain during the evolution of a normal fault population. Journal of Structural Geology 24, 1215–1231.
Morley, C.K., Harayana, C., Phoosongsee, W., Pongwapee, S., Kornsawan, A., Wonganan, N., 2004. Activation of rift oblique and rift parallel pre-existing fabrics during extension and their effect on deformation style: examples from the rifts of Thailand. Journal of Structural Geology 26, 1803–1829.
Peacock, D.C.P., Sanderson, D.J., 1991. Displacements, segment linkage and relay ramps in normal fault zones. Journal of Structural Geology 13, 721–733.
Platel, J.P., Roger, J., 1989. Evolution géodynamique du Dhofar (Sultanat d'Oman) pendant le Crétacé et le Tertiaire en relation avec l'ouverture du golfe d'Aden. Bulletin de la Societe Geologique de France 2, 253–263.
Reches, Z., 1978. Analysis of faulting in three dimensional strain field. Tectonophysics 47, 109–129.
Reches, Z., 1988. Evolution of fault patterns in clay experiments. Tectonophysics 145, 141–156.
Schlische, R.W., Withjack, M.O., Eisenstadt, G., 2002. An experimental study of the secondary deformation produced by oblique-slip normal faulting. AAPG Bulletin 86, 885–906.
Schumacher, M.E., 2002. Upper Rhine Graben: role of preexisting structures during rift evolution. Tectonics 21. doi:10.1029/2001TC900022.
Sinclair, I.K., 1995. Transpressional inversion due to episodic rotation of extensional stresses in Jeanne d'Arc Basin, offshore Newfoundland. In: Buchanan, J.G., Buchanan, P.G. (Eds.), Basin Inversion. Geological Society Special Publication, vol. 88, pp. 249–271.
ten Grotenhuis, S.M., Passchier, C.W., Bons, P.D., 2002. The influence of strain localization on the rotation behavior of rigid objects in experimental shear zones. Journal of Structural Geology 24, 485–499.
Tron, V., Brun, J.-P., 1991. Experiments on oblique rifting in brittle-ductile systems. Tectonophysics 188, 71–84.
Trudgill, B., Cartwright, J., 1994. Relay-ramp Forms and Normal-Fault Linkages, Canyonlands National Park, Utah. In: Geological Society of America Bulletin, vol. 106, pp. 1143–1157.
Walsh, J.J., Nicol, A., Childs, A., 2002. An alternative model for the growth of faults. Journal of Structural Geology 24, 1669–1675.
Walsh, J.J., Watterson, J., 1987. Distributions of cumulative displacement and seismic slip on a single normal fault surface. Journal of Structural Geology 9, 1039–1046.
Weijermars, R., 1986. Flow behaviour and physical chemistry of bouncing putties and related polymers in view of tectonic laboratory applications. Tectonophysics 124, 325–358.
Withjack, M.O., Callaway, S., 2000. Active normal faulting beneath a salt layer: an experimental study of deformation patterns in the cover sequence. AAPG Bulletin 84, 627–651.
Withjack, M.O., Jamison, W.R., 1986. Deformation produced by oblique rifting. Tectonophysics 126, 99–124.
Withjack, M.O., Schlische, R.W., 2006. Geometric and experimental models of extensional fault-bend folds. In: Buiter, S.J.H., Schreurs, G. (Eds.), Analogue and Numerical Modelling of Crustal-Scale Processes. Geological Society (London) Special Publication, vol. 253, pp. 285–305.